Force-Sensor-Based Surface Recognition With Surface-Property-Dependent Walking-Speed Adjustment of Humanoid Robot

SANDIP BHATTACHARYA [1], **AIWEN LUO** [1,2], **(Member, IEEE),**
SUNANDAN DUTTA [1], **MITIKO MIURA-MATTAUSCH** [1], **(Fellow, IEEE),**
AND HANS JÜRGEN MATTAUSCH [1], **(Senior Member, IEEE)**

[1] HiSIM Research Center, Hiroshima University, Hiroshima 739-8530, Japan
[2] College of Information Science and Technology, Jinan University, Guangzhou 510000, China

Corresponding author: Sandip Bhattacharya (sbhisim@hiroshima-u.ac.jp)

ABSTRACT We report the development of a biped-robot system with real-time surface recognition and walking-speed adjustment to control the robot motion during walking on different types of surfaces. Four types of test surfaces (i.e. rough foam (RF), smooth foam (SF), thin carpet (TC) and smooth table (ST)) are considered in the system verification. For surface-property recognition we use ultra-thin-membrane force sensors, mounted under the robot feet, and a classification circuit, implemented on an Arduino Uno board. The walking-speed adjustment is performed with an external control circuit, which receives the surface-recognition signal from the classification circuit and sends a feedback signal to the robot controller (i.e. RCB-4HV) for adjusting the walking speed accordingly. We applied the nearest-neighbor-classification algorithm with the Euclidean-distance measure and a set of reference data, to distinguish between the four test surfaces based on the robot's real-time walking pattern. The mean absolute value (MAV) feature descriptor is used to generate four different types of reference walking pattern, corresponding to the four different surfaces. In our experiments it is observed, that the ST surface performs best in terms of average surface-recognition latency (SRL) (∼3.6 sec) during walking on same surface. On the other hand, the surface transition from TC to SF showed minimum surface-transition latency (STL) (∼8.2 sec) with correct speed change from 135 to 160 robot-motor-configuration frames per stride (frames/stride), while the transition from SF to TC surfaces showed maximum STL (∼11.6 sec) including speed change from 160 to 135 frames/stride. The obtained results are useful for development of the next generation of surface-recognition and speed-adjustment systems, implemented in humanoid robots to enable balanced and stable walking in environments with multiple changed surface properties.

INDEX TERMS Humanoid robot, force sensor, microcomputer, Euclidean distance, application specific motion file (ASMF).

I. INTRODUCTION

ADVANCED surface-detection systems with corresponding speed adjustment, during humanoid-robot walking on different surfaces with controlled and stable motion, require multi-modal sensory data to safely interact with unknown real-world environments, i.e., to take correct decisions and to properly act in an autonomous way. Most of the sensor based humanoid robot interaction systems have been

The associate editor coordinating the review of this manuscript and approving it for publication was Alba Amato.

investigated using visual and auditory sensors [1]. However, the information obtained with visual and auditory sensors sometimes shows ambiguities due to the shortage of actual contact information. To receive exact contact information, the interactions between tactile sensors and real-world environments are necessary, in particular for surface recognition and corresponding decisions (e.g. speed-adjustment). The contact information depends on the surface type (e.g. example hard, soft, smooth and rough etc.), which can be extracted by using tactile sensors. Hence, tactile sensors can be expected to substantially strengthen the real-world surface recognition and

S. Bhattacharya *et al.*: Force-Sensor-Based Surface Recognition With Surface-Property-Dependent Walking-Speed Adjustment

IEEE *Access*

the self-balancing motion- control capabilities of humanoid robots [1]. In general, the tactile sensors have drawn a greater attention from all robotics-research communities, due to the necessity of acquiring the provided contact-force information for targeted processing of such information. Over the last couple of years, an enormous number of tactile sensors have been developed for surface recognition, as reported in [1]–[4]. The force/torque sensor is a special kind of tactile sensors, which is used for surface recognition, as reported in [5]–[8]. The capacitive types of tactile sensors are used in biped robots to measure the ground-contact force (GCF) and classify the surfaces with more than 90% accuracy, as reported in [9]. Most of the previous research work focused firstly on the tactile-sensing-hardware constituents of tactile sensors and the associated electronic-processing interface for the sensor-collected raw information. The second focus were the computational information-processing tools, using different artificial-intelligence-based algorithms (e.g. ANN, SVM, AdaBoost, random forest, unsupervised learning etc.), that help to construct real-world models for classifying different surfaces (e.g. material, texture classification etc.) by extracting the essence of raw tactile-sensor information. On the other hand, very limited numbers of research studies, targeting the self-balancing of humanoid robots with suitable control mechanisms during autonomous dynamic walking on different surfaces, have been reported. Research based on a control architecture with stabilizers for stable 3D dynamic walking of a biped robot on compliant contact environments has been reported in [10]. The simulation-based dynamic stable walking of a humanoid robot with a control architecture has been reported in [11]. A novel feed-back control method, called Dynamic Balancing Force Control (DBFC), is used in [12] to perform several tasks with self-balancing under an unknown perturbation. Shuuji Kajita *et al.* reported a novel balance-control method for a humanoid robot using a force-contact torque controller, which constitutes good back-drivability and a feedback-control mechanism during dynamic walking [13]. A stabilizer-based viscoelastic reaction-mass pendulum model for dynamic balancing and motion control of a humanoid robot (HRP-2), without using contact-force sensors has been reported in [14], [15]. Some recent research work, based on a whole-body-framework control during dynamic motion of the biped robot uses contact force/moment control, as reported in [16]. The main approach in [16] is to maintain the dynamic balance of torque-controlled robots by adjusting contact force and moment through the application of a null-space torque-control algorithm, which was implemented on the humanoid robot's leg. Linear model predictive control is a special kind of control mechanism, which allows stable walking of the humanoid robot in the presence of strong disruptions on the surface. This control model is implemented in the HRP-2 humanoid robot, reported in [17].

Motivated by the previous works, we have implemented a low-cost, flexible and hardware-efficient surface-recognition and dynamic speed-adjustment system for humanoid robots,

based on force sensors and external control circuitry. In our experiments, we used four different types of test surfaces for detection during robot walking. The developed dynamic surface-detection and speed-adjustment system, as illustrated in Fig. 1, consist of the Kondo KHR-3HV humanoid robot [18], two thin and flexible force sensors [19] attached under the robot feet, microcomputer-1 (i.e. Arduino-UNO board) used for raw sensor-data processing, microcomputer-2 (i.e. robot-controller RCB-4HV) for controlling the robot motion dynamically and finally, an external control circuit to control the robot motion dynamically by accessing the decision signal from microcomputer-1. To recognize different flat surfaces during real-time humanoid-robot walking on these surfaces, we extract feature vectors from the force-sensor-generated raw data and use the Euclidean-distance calculation to search the closest neighbor among given reference vectors to generate the corresponding decision signal.

FIGURE 1. Overall Proposed system level architecture for surfaces recognition and dynamic walking-speed adjustment on different surfaces using humanoid robot, force sensors and external control circuits. (b) Schematic view of Humanoid robot Kondo KHR-3HV and piezo-resistive force sensors.

The paper is organized as follows. Section II describes the related work. Section III describes the robot-system development for real-time surface-recognition and speed adjustment during dynamic walking. Section IV describes the experimental setup. Section V describes surface recognition and decision-signal generation, followed by the results presentation and discussion in Section VI. The conclusions are drawn in Section VII.

II. RELATED WORK
In this section, we described previous related research findings on walking-speed adjustment of humanoid robots during walking on different walking terrains. In [20], a method for

IEEE *Access*

S. Bhattacharya *et al.*: Force-Sensor-Based Surface Recognition With Surface-Property-Dependent Walking-Speed Adjustment

walking speed improvement without changing the reduction ratio at the robot's joint-motor system is reported for different surface conditions, using the Bonten-Maru II humanoid robot. In their experiment, the authors have worked with both simulation approaches and experimental measurements, to verify performance improvements. A comparative study based on walking-speed transition for both humans and humanoid robots with controllable stiffness and limb coordination is reported in [21]. In this work, it is demonstrated, that variable stiffness and limb coordination are important for adaptive human walking, and that implementation of these concepts can also improve the performance of a bipedal walking robot. Gait generation inspired by human behavior and related walking-speed control for humanoid robots, using a neural oscillator and an evolutionary algorithm (MLP), is reported for different walking surfaces in [22]. The authors have suggested, that their present research result is more accurate for smooth walking-speed transition between surfaces, than earlier results. A novel hierarchical control strategy for biped-robot walking on uneven terrain is reported in [23]. In this work, authors have considered a blind humanoid robot, walking on uneven terrain with high walking speed, which may generate a huge foot-contact force. Using their control strategy, the foot-contact impact can be reduced. Thus, the robot can walk blindly with fast walking speed and high reliability on an uneven terrain.

III. ROBOT-SYSTEM DEVELOPMENT

The proposed system is developed for dynamical surface detection and speed adjustment during humanoid-robot walking on different surfaces to enable stable movement with the help of force sensors, microcomputers and an external control circuit.

Figure.1 illustrates the system-level architecture of our developed biped-robot system, which recognizes the walking-surface types using force sensors and adjusts the walking speed during transition from one surface to another surface, in order to prevent robot falling and improve walking stability.

The Kondo KHR-3HV humanoid robot [18] is used for our ongoing experiments. It includes 17 active servomotors and an RCB-4HV microcontroller. Height and weight of the robot are 40.11 cm and 1.5 kg, respectively.

The force sensors form a major part in this system and are mounted under the robot feet, to extract raw sensor data for enabling surface-type detection and robot-speed adjustment. The total active area of each of the piezo-resistive force sensors is 39.6 × 39.6 mm [19].

The classification unit is another important part in this system, applied for raw-sensor-data processing with an ATmega328P microcontroller, which is attached into an Arduino-UNO board (i.e. Microcomputer-1). Hardware-compatible-embedded programming is used to design the classification unit, so that it can recognize the exact walking surface using force-sensor data and further can generate a decision signal in the form of an analog voltage.

The external control circuit contributes the active role of dynamically adjusting the robot's walking speed during walking on different surfaces. It applies 4 different colors of LEDs, 4 operational amplifiers (LM358) and a 16-channel analog multiplexer (i.e. TC9152P) [24]. This external controller circuit receives a pulse-width-modulation (PWM) signal as the decision-signal from the classification unit and provides the feedback to the AD-port of the robot controller (RCB-4HV) in the form of a stable analog voltage (i.e. constant DC voltage), to control the robot's walking speed when the robot is moving from one surface to another surface.

In this work, we mainly focused on the system development for high-accuracy real-time surface recognition and appropriate speed adjustment, when the robot is walking on changing surfaces.

IV. EXPERIMENTAL SETUP
A. TYPES OF TEST SURFACES

Test-surface selection for humanoid-robot walking is a vital part for verification of the system development. Some surface related recent work was reported in [3]–[8]. The proposed experimental setup involves the following four types of surfaces, where the robot can walk smoothly without falling (see Fig.2 (left-side)).

- S-1: rough foam (RF)
- S-2: smooth foam (SF)
- S-3: thin carpet (TC)
- S-4: smooth table (ST)

Due to surface-property variations in smoothness, roughness or softness, the sensor-detected voltage also varies during robot walking as shown in Fig.2 (right-side). Rough-foam, smooth-foam, thin-carpet and smooth-table surfaces have a thickness of 0.9 cm, 0.9 cm, 0.3 cm and 3.5 cm, respectively. In every experimental run, we set the humanoid robot to walk on each of the four surfaces individually and collected the force-sensor data for surface-pattern recognition and corresponding decision-signal generation for dynamic speed adjustment of the humanoid robot. From Fig.2, it is observed that the sensor-detected voltage responses show surface-related variations during robot walking. These voltage-pattern variations are useful for surface recognition and walking-speed control.

B. PIZO-RESISTIVE FORCE SENSORS

Advanced tactile sensors have been widely used for surface recognition in several robotics applications. Some latest tactile sensors for surface recognition are reported in [1]–[4]. The force sensors are a special tactile-sensor kind, which are attached under the robot feet to measure the robot-weight-induced foot-contact force in the form of an analog voltage with a suitable sampling rate [19]. In our measurement setup, we used low-cost, thin and flexible piezo-resistive-membrane force sensor (see Fig.1) with analog-type force resolution and 39.6 × 39.6 mm active area. Working range is 0~5V with <1ms response time, to measure the foot-contact force of
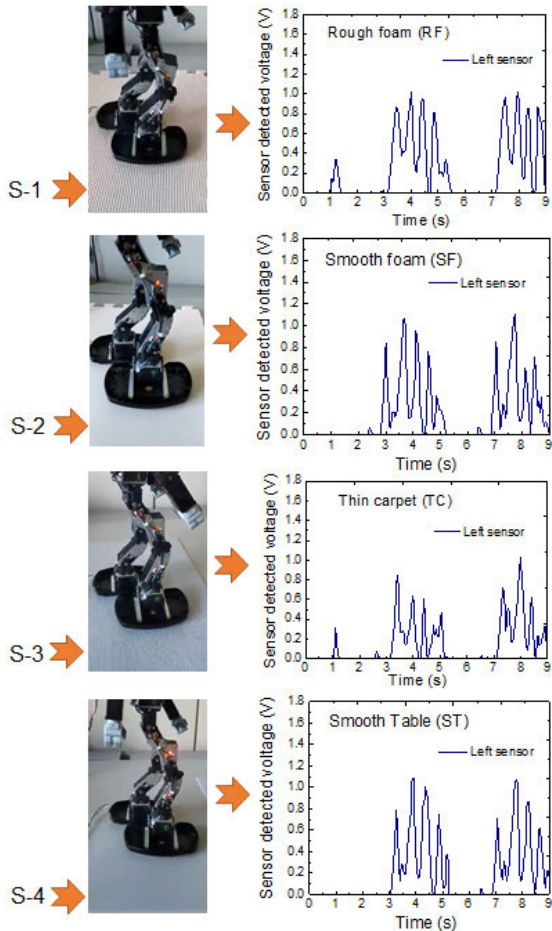
FIGURE 2. Left-side: Schematic representation of robot walking on four different types of surfaces (rough foam (RF), smooth foam (SF), thin carpet (TC), and smooth table (ST)). Right-side: Left-foot-sensor-detected raw data in the form of an analog voltage during walking on the different surfaces.

the robot during walking on different surfaces. Force-sensor-generated raw-voltage data are sent to the classification unit, implemented on microcomputer-1 (see Fig.3 (a)), for fast dynamic surface-property recognition and generation of a decision signal in the form of an analog voltage to adjust the walking speed.

C. MICROCOMPUTERS

Microcomputers are major building blocks in our experimental setup. We use two different microcomputer types, as explained below in detail.

- **Microcomputer-1**: The microcomputer-1 is basically an Arduino-UNO open-platform board, which consist of an 8-bit microcontroller (i.e. ATmega328P), implemented by CMOS technology with RISC architecture and 32k Bytes on-chip flash memory. It is used to collect the raw analog data from the piezo-resistive-membrane force sensors during humanoid-robot walking on different surfaces and to process those data for surface recognition with a software-implemented classification
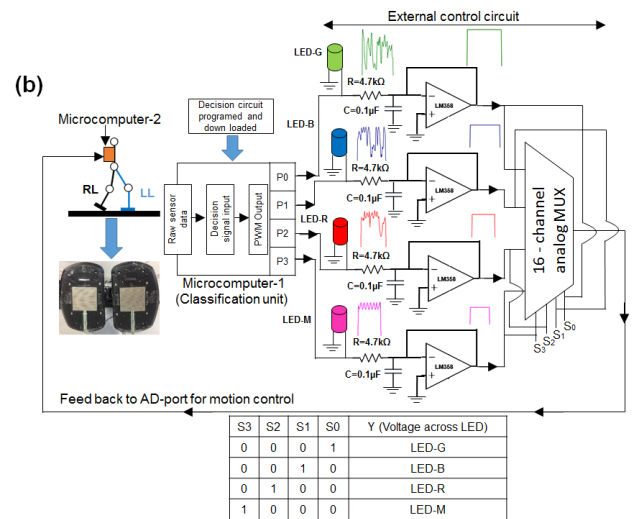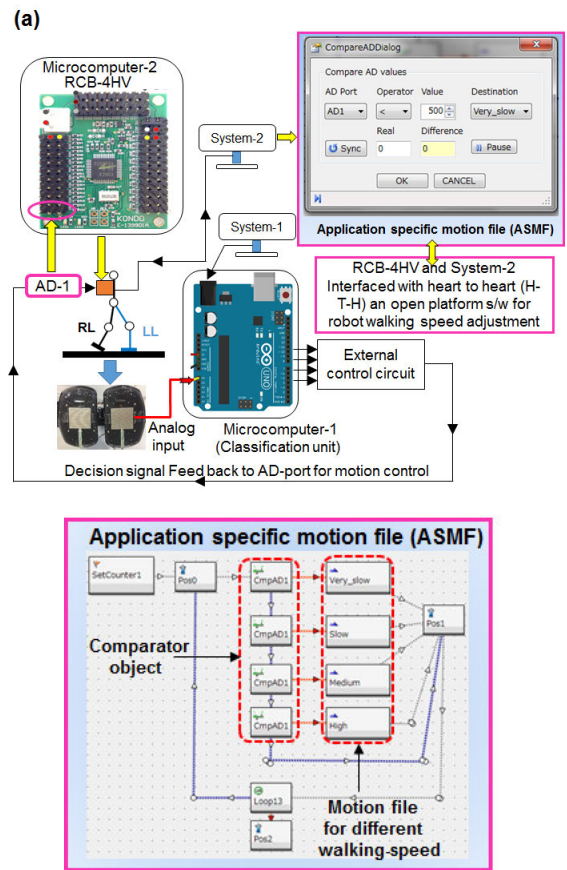
FIGURE 3. (a) Full experimental setup for surface detection and speed control during humanoid-robot walking on different surfaces. (b) Details of External control circuit for online speed adjustment (used components: four different colored LEDs, four RC-low pass filters, four operational amplifiers and one 16-channel analog multiplexer).

unit. The classification-unit output is then used to generate a decision signal in the form of an analog voltage across the LEDs. Classification-unit implementation on the ATmega328P microcontroller uses embedded programming by employing an integrated development environment (IDE) on system-1 (see Fig.3 (a)).

IEEE *Access*

S. Bhattacharya *et al.*: Force-Sensor-Based Surface Recognition With Surface-Property-Dependent Walking-Speed Adjustment

- **Microcomputer-2**: The microcomputer-2 is another important component in our experimental setup. It is functioning as a robot controller (i.e. RCB-4HV), embedded with a single-chip microprocessor-control unit (MCU) (i.e. M30260F8AGP) and fabricated using high-performance CMOS technology with 68k Byte internal memory (i.e. flash type). It also contains a 12-channel, 10-bit A/D converter, which is used for the decision-signal feedback coming from the classification unit (see Fig.3 (a)). The RCB-4HV board is interfaced with the robot-controlling software and uses the application specific motion file (ASMF) through which the robot can change the dynamic motion during walking (see Fig.3 (a)). The AD-port of RCB-4HV receives only one decision signal (i.e. analog voltage) at a time, coming from the output terminal of the external control circuit. After AD-conversion, it is transferred to the software-driven ASMF (see Fig. 3 (a)), containing four object-oriented comparators, which compare the four surface-specific decision signals, generated as voltage-drops across LEDs, separately. Each decision signal for the surface recognition is compared with all four comparators. If the online decision signal matches with the assigned reference values, stored in the comparator objects, then the main motion file will call the speed-change object (i.e. very slow, slow, medium and high) to appropriately adjust the robot-motion speed during transitions between surfaces (see Fig. 3 (a)).

D. EXTERNAL CONTROL CIRCUIT FOR SPEED ADJUSTMENT

Surface recognition and speed adjustment are primary tasks of any advance robot controller for adjusting the walking speed autonomously and to obtain dynamic balancing features. The external control circuit plays an active role for the change of the walking speed by identifying the exact surface pattern and is functioning as an intermediator between microcomputer-1 (i.e. Arduino-UNO) and microcomputer-2 (i.e. RCB-4HV), for walking-speed adjustment when the robot crosses between surfaces, as illustrated in Fig.1 and Fig.3 (b). To design the external controller circuit, we used four resistors (R=4.7kΩ), four electrolyte-type capacitors (C=0.1pF) with operating-voltage rating of 50V, as well as four low-power operational amplifiers (LM358) with 1MHz bandwidth and wide power-supply range (3-32 V). Further, we applied one low-power CMOS-based 16-channel analog multiplexer (TC9152P) with wide operating-voltage range (5-32) and four different colored LEDs to generate the analog-voltage drops corresponding to the decision signal, as illustrated in Fig.3 (b). The RC networks are functioning as passive low-pass filters to remove unwanted voltage fluctuations of the decision signal due to robot-motor-generated noise across the LED terminals, resulting from mechanical robot-body oscillations during dynamic walking, as illustrated in Fig.3 (b) and Fig.4. The outputs from the four RC filters are connected
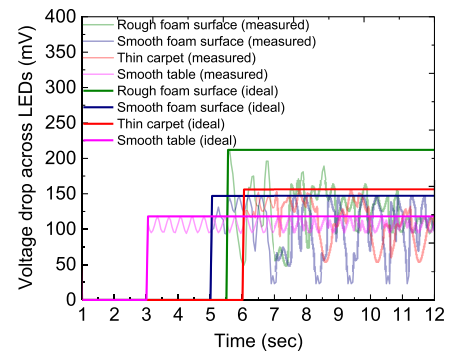
FIGURE 4. Measured decision signals across the LEDs, including the maximum peak voltages. We obtained max-peak values of 212 mV, 147 mV, 156 mV and 118 mV for rough-foam, smooth-foam, thin-carpet and smooth-table surfaces, respectively.

to four unity-gain-buffer circuits (i.e. operational amplifiers) to retain constant DC levels without voltage shifts, because the RCB-4HV board needs constant voltage levels for reliable recognition. These voltage levels are assigned in the robot operating software (i.e. the H-T-H software-specific motion file, also referred to as ASMF) (see Fig.3 (a)). The four operational-amplifier outputs are connected to the input terminals of the 16-channel analog multiplexer, which selects one of the four voltage inputs (i.e. the decision signal) for connection to the input terminal (i.e. AD-port) of the robot controller (i.e. the RCB-4HV board). Similarly, the robot operating software (i.e. the H-T-H software) compares the decision signal from the AD-port by using the comparator object (i.e. the software-driven ASMF) and decides the robot-motion speed according to the corresponding recognition result. When the classification part in Fig.3 (b) recognizes that the robot is walking on a rough-foam surface, only the green color LED will be activated to glow and the voltage drop across this LED ($\sim$212mV) will be transferred to the output of the multiplexer by choosing the select line S_0 = high. Similarly, for smooth-foam, thin-carpet and smooth-table surfaces, the corresponding blue, red or magenta LED will be activated to glow and the respective voltage drop ($\sim$ 147mV, $\sim$156mV or $\sim$118mV) will be transferred to the output of the multiplexer by activating the S_1, S_2 or S_3 line. The output terminals of the four operational amplifiers can be directly connected with S_0, S_1, S_2, and S_3 for the selection purpose, because the voltage drops across the LEDs are sufficient for activating the corresponding analog-multiplexer port.

E. DATA COLLECTION

The force-sensor-generated raw-data collection is one of the elementary tasks during robot walking on different surfaces, to recognize the surface pattern and adjust the walking speed. In our experiment, we collected a large amount of serial raw-sensor data online, using the Arduino UNO board (i.e. microcomputer-1), which were then segmented offline into the corresponding robot-walking steps. Each walking step
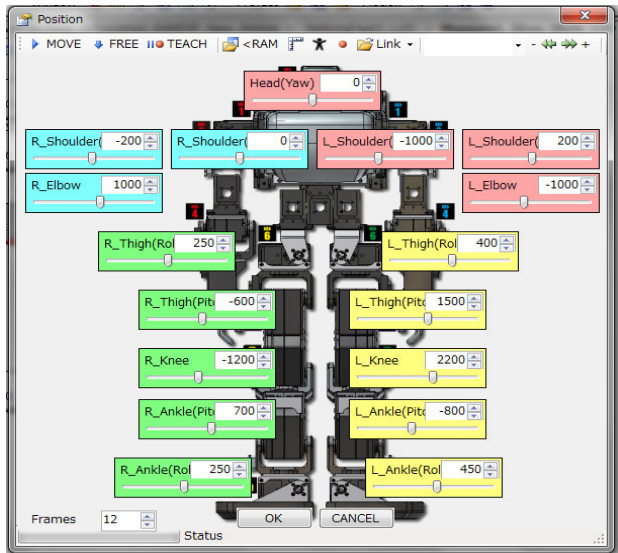
FIGURE 5. Motor design specification with assigned frame number and angle of rotation for all 17 servomotors (H-T-H s/w supported GUI).

TABLE 1. Adjusted parameters during robot walking.

Sampling time, T_S=50 ms/point with frame rate, f_{RATE} =20 ms/frame			
Sampling point (speed)	T_P (sec)	V_{SPEED}^{-1} (frames/ stride)	Surfaces
M=76 (very-slow)	3.8	190	Rough foam
M=64 (slow)	3.2	160	Smooth foam
M=58 (medium)	2.7	135	Thin carpet
M=50 (high)	2.5	125	Smooth table

ignored until the robot walking became stable, and then we collected the offline reference data for surface recognition by nearest neighbor search. For feature extraction, we used the mean absolute value (MAV) feature descriptor, which is sufficiently simple and has low computational cost. The feature-vector construction for surface recognition, subsequent decision-signal generation and the walking-speed adjustment are explained in the following Section IV.

V. SURFACE RECOGNITION AND DECISION SIGNAL GENERATION

The dynamic surface recognition during walking on different surfaces is one of the challenging tasks for a humanoid robot. For the surface recognition, the feature extraction from the raw sensor data is one of the crucial steps, which should allow distinguishing the four different surface types even in the presence of noisy force-sensor data. There are several ongoing research studies based on pattern recognition using different types of feature vectors to distinguish different types of surfaces. Some work related to feature-extraction algorithms was reported in [25]–[31]. In our experiments, we used the mean absolute value (MAV) feature, to simplify the calculation and to reduce the information-processing cost. The sliding window algorithm, implemented on the ATmega328 microcontroller, is used to generate the MAV feature [30], [31] (see Fig.6). For real time pattern matching we use the Euclidean-distance-search algorithm with the k-nearest neighbor (kNN) classifier [32]–[34] to match the online pattern dynamically with the most similar reference pattern (see Fig.6). The MAV feature calculating equation is

$$MAV = \frac{1}{N} \sum_{i=1}^{N} x_i \qquad (3)$$

where, N (in our case chosen as N=M/2) and xi denote the sliding-window size and the raw sensor-data points, respectively. For online MAV feature generation, the window slides online over the raw input data, transmitted serially from the force sensor. The generated MAV feature represents therefore the dynamic results from a mathematical convolution operation between the sliding window and the raw force-sensor data [31]. In our analysis, we used four different test surfaces, for which corresponding MAV reference features are shown in Fig. 6 with four different colors (i.e. green, blue, red and magenta). These green, blue, red and magenta colored features represent offline MAV-reference data for rough-foam, smooth-foam, thin-carpet and smooth-table surfaces. The Euclidean distance is used for determining the nearest
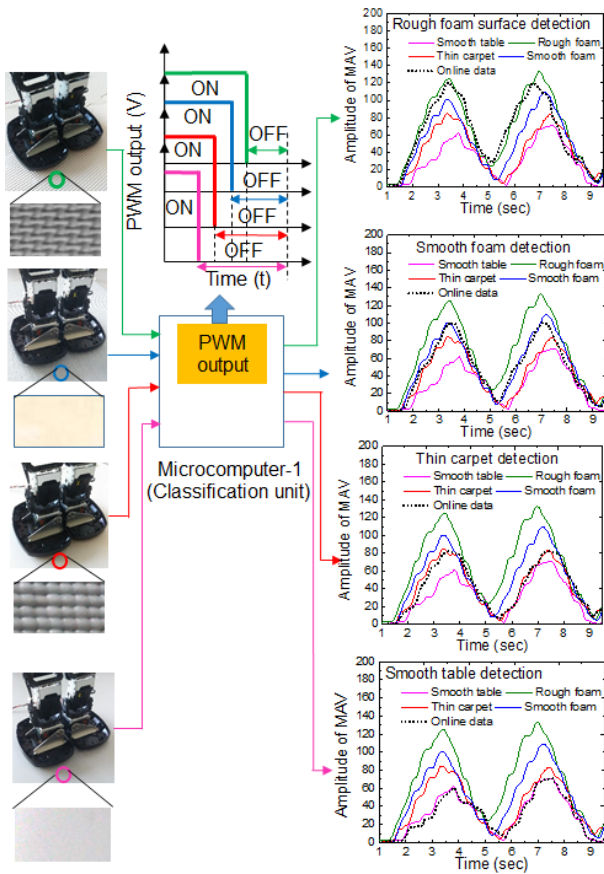
represents one walking-reference sample or stride (see Fig.1), consisting of M (M>0) raw sensor-data points. During the data extraction process, two consecutive raw sensor-data points are separated by 50 ms. The sampling rate TS is therefore 50 ms/point, which can in principle be adjusted by embedded programming (10ms $\geq$ T_S <1000ms). So, the total time T_P required to cover the sample period of one stride can be represented as

$$T_P = M \times T_S \qquad (1)$$

The number of sensor-data points per stride M is a variable parameter, which depends on robot walking speed and is M equal 76, 64, 58, and 50 for very slow, slow, medium, and fast speeds, respectively, at a fixed sampling rate of. TS = 50 ms/point. The walking speed of the humanoid robot is related to the number of frames (i.e. robot-motor configurations) per stride, which is determined in the robot-design specification. It can be adjusted by changing the mechanical parameter for the robot motors, such as the fixed angles of rotation in the robot-operating software (see Fig. 5). Each frame represents in principle a static posture of the humanoid robot during its motion, while the frame rate f_{RATE} defines the delay time for changing between two subsequent robot postures. In our experiments, we considered f_{RATE} = 20 ms/frame. So, the humanoid robot's walking speed can be related to the frame number per stride in the following form

$$V_{SPEED}^{-1} = \frac{T_p}{f_{RATE}} \qquad (2)$$

By using above equation, the robot's walking speed can be adjusted by changing the number of motor-configuration frames per stride and therefore the number of sampling points per stride, as illustrated in Table 1. In our experiment, we used the walking-speed adjustments given in Table 1 for our 4 different test surfaces. During reference-data collection for the different surfaces, the first few strides were

IEEE *Access*

S. Bhattacharya *et al.*: Force-Sensor-Based Surface Recognition With Surface-Property-Dependent Walking-Speed Adjustment

offline-reference feature to the online MAV-feature, generated dynamically from the raw force-sensor data and shown by the black dotted line in Fig.6 [35]. When the robot is walking on different surfaces in real-time, the corresponding offline-reference pattern and online-walking pattern are close to each other. For example, when robot is walking on a rough-foam surface, the green colored MAV feature and the online black-dotted line are closest to each other. The hardware-accelerated classification unit generates the decision signal in the form of a pulse width modulation (PWM) output. Since the amplitudes of the MAV features for all surfaces are different, the PWM-signal widths are also different (see Fig.6). The corresponding duty cycles of the PWM signals for all different recognized surfaces are listed in Table 2. Maximum duty cycle corresponds to maximum detection time (i.e. glowing time) across the LEDs. The generated PWM signals are connected with the four corresponding colored LEDs, to display the recognition results of the different surfaces visually. The voltage drops across the colored LEDs are different due to their illumination properties (i.e. different frequency) (see Fig.7). These voltage
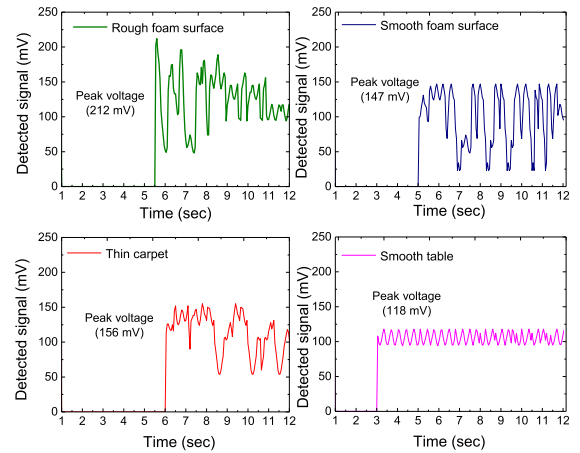
drops across the LEDs serve as feedback to the robot controller (RCB-4HV board) via the external controller circuit to dynamically change the robot motion when a transition from one surface to another surface is detected. The obtained results for surface recognition and robot-speed adjustment will be presented in the next section.

VI. RESULTS AND DISCUSSION

Here, we discussed the experimental surface-recognition and speed-adjustment results for humanoid-robot walking on different types of surfaces. We separately analyze the experimental surface-recognition results for robot walking on the same surface and for a transition between walking surfaces. Concerning the walking-speed adjustment, we considered only the transition between surfaces. Figure 8 illustrates the surface-recognition-latency (SRL) measurements, when the robot is walking on the four different surface types. Here, S1 to S4 represent the initial walk-starting time and R1 to R4 represent the surface-recognition time by the humanoid robot of the four different surfaces. The differences between the walk-starting times (S1 to S4) and the recognition times (R1 to R4) represent the respective surface-recognition latencies ($\Delta T1$ to $\Delta T4$). These latencies are different for the different surface types, due to the different material properties (e.g. softness, hardness) of the used surfaces.

A. SURFACE RECOGNITION (WALKING ON THE SAME SURFACE)

For humanoid-robot walking on the same surface, reliable surface recognition and short recognition latency are important tasks during recognition-system development. To confirm correct recognition and to measure surface-recognition latency on the same surface (SRL-SS), we used 50 experimental test runs with four walking speeds for each surface (see Table. 1). Correct surface recognition was
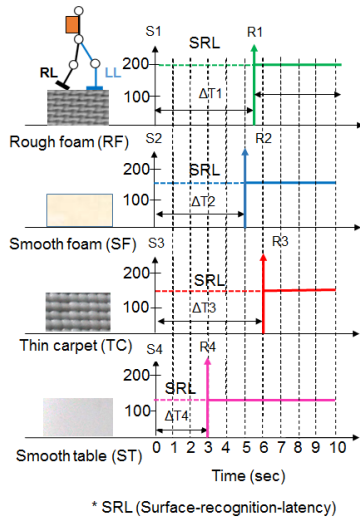
S. Bhattacharya *et al.*: Force-Sensor-Based Surface Recognition With Surface-Property-Dependent Walking-Speed Adjustment

IEEE Access

FIGURE 8. Schematic representation of surface-recognition-latency (SRL) determination for the four different surface types, where ΔT1 to ΔT4 represent the time delay between initial walk-starting times (S1 to S2) and surface-recognition times (R1 to R4) of the robot.

TABLE 2. PWM-signal generation for different surfaces.

Sampling time, T_S=50 ms/point, T_P (sec) =3.8, V_{SPEED} =190 frames/ stride and frame rate, f_{RATE} =20 ms/frame, total period = 2.6 sec			
Surfaces	I_{ON} (sec)	I_{OFF} (sec)	Duty Cycle = $\dfrac{I_{ON}}{I_{ON}+I_{OFF}}$(%)
Rough foam	1.82	0.78	70.00
Smooth foam	1.45	1.15	55.76
Thin carpet	1.23	1.37	47.30
Smooth table	1.09	1.51	41.92

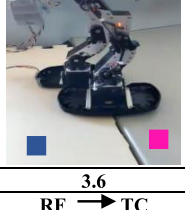electrical signals, which obviously leads to a speed-up of the recognition time.
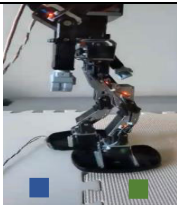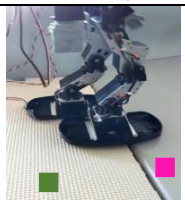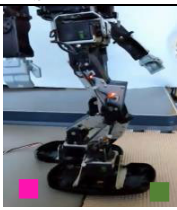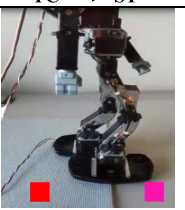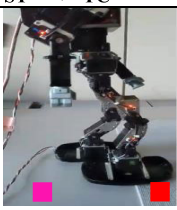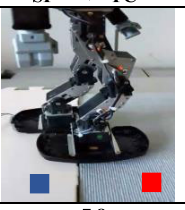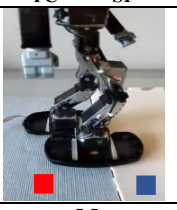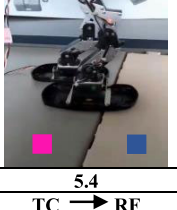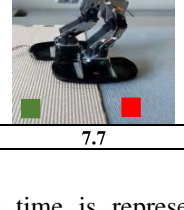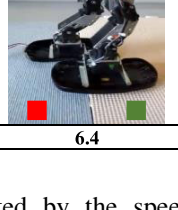
B. SURFACE RECOGNITION (TRANSITION BETWEEN SURFACES)

When the robot is transitioning between surfaces during walking, surface-recognition latencies of the new surface after surface transition (SRL-ST) are found to be quite similar to the case of walking on the same surface. We have measured the 12 possible combinations for transitions between the four different surfaces with 100 experimental runs for each combination. Table 3 shows these possible surface-transition combinations and also lists the average of the measured surface-recognition latencies for the new surfaces after surface transition (SRL-ST). The different colors correspond to the colors of the LEDs, across which the surface-specific decision signal is generated. A comparison of the results for the average surface-recognition latencies after the surface transitions is illustrated in Table 4. It can be seen that, when the robot walks from a TC, SF or RF surface to a ST surface, the average surface-recognition latency (SRL-ST) (∼3.5-3.6 sec) is shorter than for other surface-transition cases, whereas the SRT-ST latency is longest (∼7.7-7.9 sec), when the robot walks from a RF, SF or ST surface to a TC surface. The above experimental results confirm that our developed walking-surface-recognition system for humanoid robots performs fastest in terms of surface-recognition latencies (SRL-ST), when the robot moves from any of the other surfaces to a ST surface. On the other hand, the recognition latencies are slowest, when the transition occurs from any of the other surfaces to a TC surfaces.

C. SPEED ADJUSTMENT

Appropriate walking-speed adjustment is another essential task during humanoid-robot transition between surfaces. For example, when the humanoid robot walks on a RF surface, it first recognizes the surface type using the MAV-feature generated from the force-sensor data and then adjusts the walking speed to 190 frames/stride, by using the decision signal (generated by classification unit) and the external controller circuit. During transition from RF to SF surfaces, the speed is adjusted to 160 frames/stride after surface recognition, requiring a speed-adjustment time (see Fig. 11). The surface-recognition time is represented by the surface-recognition latency for surface transition (SRL-ST) and

verified in all tests and the surface-recognition latency varied for different surfaces, due to variations in the time for decision-signal generation. In particular, we observed that the surface-recognition latency is shortest for ST surfaces with an average of 3.6 sec and longest for TC surfaces with an average of 7.9 sec (see Fig.9). Further, our experimental results indicate that the humanoid robot can recognize the smoother surfaces (ST and SF) with less surface-recognition latency than the rougher surfaces (RF and TC).
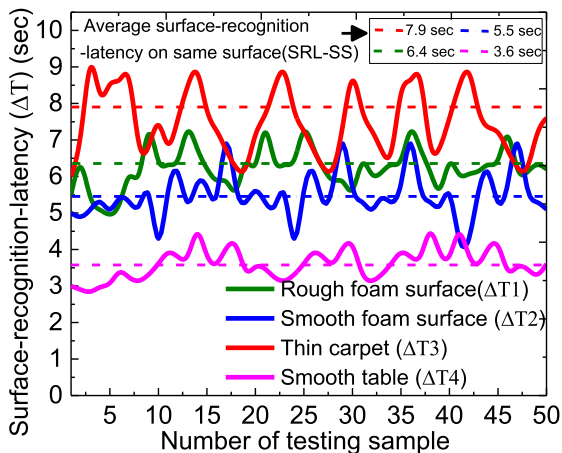
FIGURE 9. Measured surface-recognition latencies during each of the experimental test runs for robot walking on the four different surfaces without surface transition.

The faster recognition of smoother surfaces in terms of surface-recognition latency is attributed to the fact that the total surface area, directly touched by the force sensors, is larger in the case of smoother surfaces. As a result, maximum mechanical forces are utilized in the conversion to

IEEE Access

S. Bhattacharya *et al.*: Force-Sensor-Based Surface Recognition With Surface-Property-Dependent Walking-Speed Adjustment

TABLE 3. Transitions between two surfaces.

	Surface transition	
	RF → SF	SF → RF
Surface-recognition-latency after surface transition (SRL-ST)		
SRL-ST (sec)	5.6	6.3
	RF → ST	ST → RF
SRL-ST (sec)	3.5	6.4
	TC → ST	ST → TC
SRL-ST (sec)	3.5	7.9
	SF → TC	TC → SF
SRL-ST (sec)	7.8	5.5
	ST → SF	SF → ST
SRL-ST (sec)	3.6	5.4
	RF → TC	TC → RF
SRL-ST (sec)	7.7	6.4

TABLE 4. Surface transition latency (STL) for transitions between different surfaces.

Surface transition	Speed transition (frames / stride)	Surface recognition latency (SRL-ST) (sec)	Speed adjustment latency (SAL) (sec)	Surface transition latency (STL) (sec)= SRL-ST (sec) +SAL (sec)
RF → SF	190 to 160	5.6	4.6	10.2
SF → RF	160 to 190	6.3	3.1	9.4
RF → ST	190 to 125	3.5	6.6	10.1
ST → RF	125 to 190	6.4	3.2	9.5
TC → ST	135 to 125	3.5	5.8	9.3
ST → TC	125 to 135	7.9	1.1	9.0
SF → TC	160 to 135	7.8	3.8	11.6
TC → SF	135 to 160	5.5	2.7	8.2
SF → ST	160 to 125	3.6	5.9	9.5
ST → SF	125 to 160	5.4	3.1	8.5
RF → TC	190 to 135	7.7	2.7	10.4
TC → RF	135 to 190	6.4	1.9	8.3

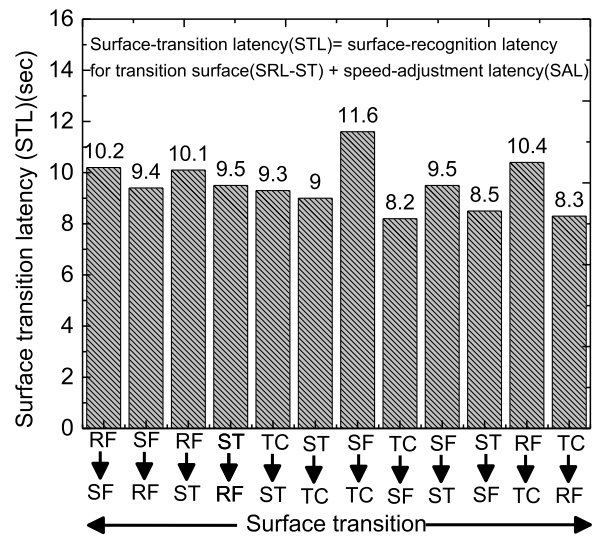**NB: RF < SF < TC < ST** (According to speed measure)

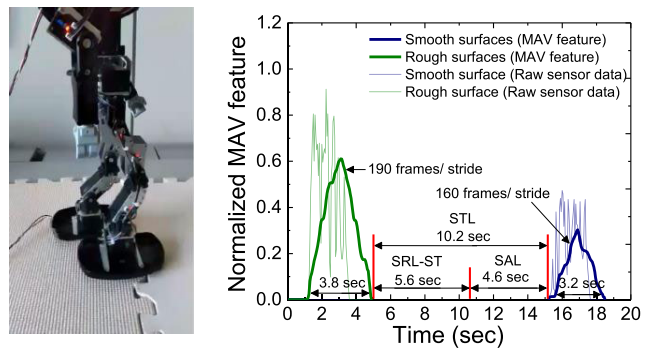**FIGURE 10.** Measured average surface-transition latencies (STL) after robot transition between surfaces.

FIGURE 11. Surface recognition and speed adjustment during transition from rough foam (RF) surface to smooth foam (SF) surfaces.

the speed-adjustment time is represented by the speed-adjustment latency (SAL) (see Fig.11). The summation of these two time intervals is denoted as the surface-transition

latency (STL). Figure 10 summarizes the STL results for all possible surface transitions. These STL results include the time from surface recognition to decision-signal feedback at
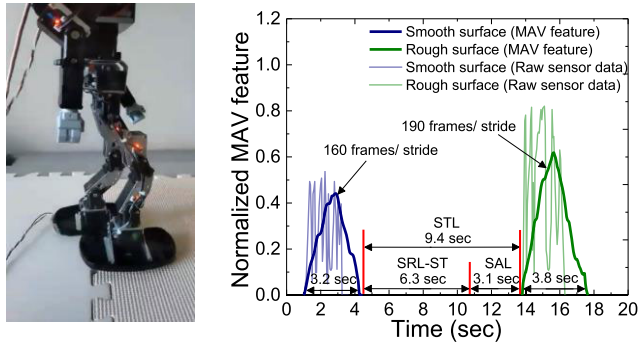
S. Bhattacharya *et al.*: Force-Sensor-Based Surface Recognition With Surface-Property-Dependent Walking-Speed Adjustment

IEEE *Access*

FIGURE 12. Surface recognition and speed adjustment during transition from smooth foam (SF) surface to rough foam (RF) surfaces.
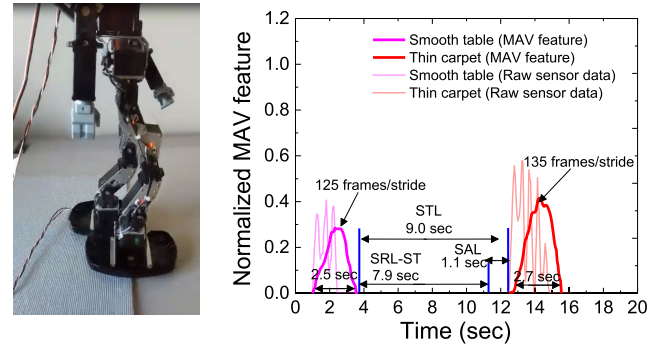

FIGURE 14. Surface recognition and speed adjustment during transition from smooth table (ST) to thin carpet (TC) surfaces.
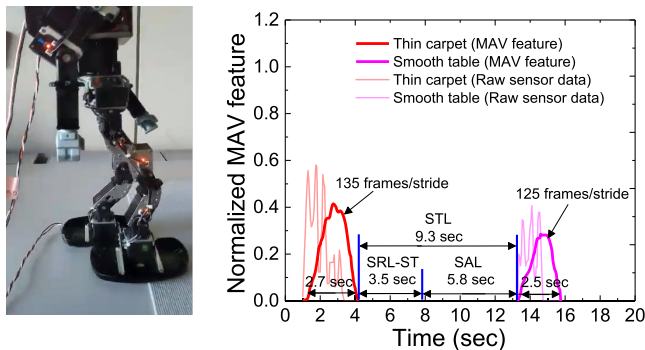

FIGURE 13. Surface recognition and speed adjustment during transition from thin carpet (TC) to smooth table (ST) surfaces.

the AD-port for walking-speed adjustment. During RF to SF surface transition, the average measured STL is 10.2 sec. In Fig.11, it is clearly observed that, when the robot is walking on RF surfaces, the time for one stride is 3.8 sec (i.e. width of the MAV feature in green color). After transition from the RF to a SF surface, the time for one stride is correctly changed from 3.8 sec (i.e. very-slow walking speed) to 3.2 sec (i.e. slow walking speed) and the corresponding MAV feature is generated (shown with blue color in Fig.11).

Similar measurements have been performed for SF to RF surface transitions, to verify the correct walking-speed adjustment (see Fig.12). In this case, the surface-transition latency (STL) becomes 9.4 sec. Figures 13 and 14 illustrate the transitions from TC to ST surfaces and vice versa with different walking speeds and different MAV-feature widths (i.e. times for one stride). It is observed that, during transition from TC to ST surfaces, the walking speed correctly changes from 135 frames/stride (i.e. medium speed) to 125 frames/stride (i.e. fast speed) with an appropriately changing MAV feature width from 2.7 sec to 2.5 sec (see Fig.13). The surface-transition-latency (STL) becomes 9.3 sec, including the change of the walking speed from medium to fast.

Similarly, we performed the surface-transition experiments from ST to TC surfaces, as illustrated in Fig.14. It is observed that the walking speed correctly changes from 125 frames/stride (i.e. fast speed) to 135 frames/ stride

(i.e. medium speed) with a surface-transition latency (STL) of 9 sec. The measured data including SRL-ST, speed-adjustment latency (SAL) and STL for all other surface-transition cases are listed in Table 4. It is verified that, for all possible surface transitions, the speed is changed correctly. For example, the STL for SF to RF surface transitions becomes 9.4 sec, with a SAL of 3.1 sec, whereas for the inverse transition from RF to SF surfaces, the STL becomes 10.2 sec, with a SAL of 4.6 sec. The basic reason for the additional 1.5 sec in SAL, during transition from RF to SF surfaces, is attributed to the necessary increase of the induced motor-driving currents and the corresponding servomotor speed (i.e. very-slow to slow speed transition). In terms of STL analysis, we observe that the transitions from TC to SF surfaces complete faster in comparison with other surface transitions, i.e., the measured surface-transition latency for this case is the shortest of all the possible surface transitions.

VII. CONCLUSION
In this work, we explored a surface-recognition and walking-speed-adjustment system, developed for humanoid robots to enable stable dynamic walking on different surfaces without falling. The raw force-sensor data and the MAV feature descriptor are used to generate reference feature vectors for the studied four different surface types. All of these reference patterns are compared with the online-generated feature vectors when the robot is walking on an unknown surface, using the nearest-neighbor-searching algorithm and the Euclidean distance to obtain the classification result for surface recognition, which is then encoded as a specific decision signal. It is observed that, the smooth table (ST) walking-pattern recognition performs better with less surface-recognition latency on the same surface, when compared with other surfaces. On the other hand, the transition from thin-carpet (TC) to smooth foam (SF) surfaces showed the minimum surface-transition latency (STL) in comparison to other surface transitions, including the correct dynamic robot-walking-speed change from 135 frames/stride to 160 frames/stride. The analysis results from our study are useful for future AI-based robot-system design, where the robot can balance itself through changes of the robot's movement speed and its motor-angle

IEEE *Access*

S. Bhattacharya *et al.*: Force-Sensor-Based Surface Recognition With Surface-Property-Dependent Walking-Speed Adjustment

adjustments for different types of surfaces, by using an external controller circuit.

REFERENCES

[1] R. S. Dahiya, G. Metta, M. Valle, and G. Sandini, "Tactile sensing—From humans to humanoids," *IEEE Trans. Robot.*, vol. 26, no. 1, pp. 1–20, Feb. 2010.

[2] A. J. Worth and R. R. Spencer, "A neural network for tactile sensing: The hertzian contact problem," *IEEE Trans. Syst., Man, Cybern.*, vol. 22, no. 1, pp. 177–182, Jan. 1992.

[3] N. Jamali and C. Sammut, "Material classification by tactile sensing using surface textures," in *Proc. IEEE Int. Conf. Robot. Autom.*, May 2010, pp. 2336–2341.

[4] P. Giguere and G. Dudek, "A simple tactile probe for surface identification by mobile robots," *IEEE Trans. Robot.*, vol. 27, no. 3, pp. 534–544, Jun. 2011.

[5] M. A. Hoepflinger, C. D. Remy, M. Hutter, L. Spinello, and R. Siegwart, "Haptic terrain classification for legged robots," in *Proc. IEEE Int. Conf. Robot. Autom.*, May 2010, pp. 2828–2833.

[6] K. Walas, D. Kanoulas, and P. Kryczka, "Terrain classification and locomotion parameters adaptation for humanoid robots using force/torque sensing," in *Proc. IEEE-RAS 16th Int. Conf. Humanoid Robots (Humanoids)*, Nov. 2016, pp. 133–140.

[7] C. Kertesz, "Rigidity-based surface recognition for a domestic legged robot," *IEEE Robot. Autom. Lett.*, vol. 1, no. 1, pp. 309–315, Jan. 2016.

[8] K. Walas, "Terrain classification and negotiation with a walking robot," *J. Intell. Robotic Syst.*, vol. 78, nos. 3–4, pp. 401–423, Jun. 2015.

[9] X. A. Wu, T. M. Huh, R. Mukherjee, and M. Cutkosky, "Integrated ground reaction force sensing and terrain classification for small legged robots," *IEEE Robot. Autom. Lett.*, vol. 1, no. 2, pp. 1125–1132, Jul. 2016.

[10] A. Chemori, S. Le Floch, S. Krut, and E. Dombre, "A control architecture with stabilizer for 3D stable dynamic walking of SHERPA biped robot on compliant ground," in *Proc. 10th IEEE-RAS Int. Conf. Humanoid Robots*, Dec. 2010, pp. 480–485.

[11] L. C. Visser, S. Stramigioli, and R. Carloni, "Control strategy for energy-efficient bipedal walking with variable leg stiffness," in *Proc. IEEE Int. Conf. Robot. Autom.*, May 2013, pp. 5624–5629.

[12] B. J. Stephens and C. G. Atkeson, "Dynamic balance force control for compliant humanoid robots," in *Proc. IEEE/RSJ Int. Conf. Intell. Robots Syst.*, Oct. 2010, pp. 1248–1255.

[13] S. Kajita, K. Yokoi, M. Saigo, and K. Tanie, "Balancing a humanoid robot using backdrive concerned torque control and direct angular momentum feedback," in *Proc. ICRA. IEEE Int. Conf. Robot. Autom.*, May 2001, pp. 3376–3382.

[14] A. Mifsud, M. Benallegue, and F. Lamiraux, "Stabilization of a compliant humanoid robot using only inertial measurement units with a viscoelastic reaction mass pendulum model," in *Proc. IEEE/RSJ Int. Conf. Intell. Robots Syst. (IROS)*, Oct. 2016, pp. 5405–5410.

[15] A. Mifsud, M. Benallegue, and F. Lamiraux, "Estimation of contact forces and floating base kinematics of a humanoid robot using only inertial measurement units," in *Proc. IEEE/RSJ Int. Conf. Intell. Robots Syst. (IROS)*, Sep. 2015, pp. 3374–3379.

[16] Y. Lee, S. Hwang, and J. Park, "Balancing of humanoid robot using contact force/moment control by task-oriented whole body control framework," *Auto. Robots*, vol. 40, no. 3, pp. 457–472, Mar. 2016.

[17] H. Diedam, D. Dimitrov, P.-B. Wieber, K. Mombaur, and M. Diehl, "Online walking gait generation with adaptive foot positioning through linear model predictive control," in *Proc. IEEE/RSJ Int. Conf. Intell. Robots Syst.*, Sep. 2008, pp. 1121–1126.

[18] Kondo-robot.com. *Kondo Kagaku Co., Ltd.* Accessed: Dec. 20, 2018. [Online]. Available: https://kondo-robot.com/product/03178

[19] taiwanalpha.com. *Taiwan Alpha Electronic Co., Ltd.* Accessed: Apr. 10, 2019. [Online]. Available: http://www.taiwanalpha.com/en/products/21

[20] H. Yussof, M. Ohka, M. Yamano, and Y. Nasu, "Analysis of human-inspired biped walk characteristics in a prototype humanoid robot for improvement of walking speed," in *Proc. 2nd Asia Int. Conf. Modeling Simulation (AMS)*, May 2008, pp. 564–569.

[21] Y. Huang, B. Chen, L. Meng, Z. Yu, X. Chen, Q. Huang, and Q. Wang, "Exploiting human walking speed transitions using a dynamic bipedal walking robot with controllable stiffness and limb coordination," in *Proc. IEEE-RAS 16th Int. Conf. Humanoid Robots (Humanoids)*, Nov. 2016, pp. 509–514.

[22] A. A. Saputra, J. Botzheim, and N. Kubota, "Walking speed control in human behavior inspired gait generation system for biped robot," in *Proc. IEEE Congr. Evol. Comput. (CEC)*, Jul. 2016, pp. 4895–4902.

[23] C. Dong, X. Chen, Z. Yu, Z. Huang, Q. Li, Q. Zhou, and Q. Huang, "A novel hierarchical control strategy for biped robot walking on uneven terrain," in *Proc. IEEE-RAS 19th Int. Conf. Humanoid Robots (Humanoids)*, Oct. 2019, pp. 140–145.

[24] *Toshiba Semiconductor Ltd.* Accessed: Jan. 1, 2020. [Online]. Available: http://www.datasheet-pdf.com/PDF/TC9152P-Datasheet-Toshiba-768779

[25] D. You, X. Wu, L. Shen, S. Deng, Z. Chen, C. Ma, and Q. Lian, "Online feature selection for streaming features using self-adaption sliding-window sampling," *IEEE Access*, vol. 7, pp. 16088–16100, 2019.

[26] M. Asghari Oskoei and H. Hu, "Myoelectric control systems—A survey," *Biomed. Signal Process. Control*, vol. 2, no. 4, pp. 275–294, Oct. 2007.

[27] T. R. Farrell, "Determining delay created by multifunctional prosthesis controllers," *J. Rehabil. Res. Develop.*, vol. 48, no. 6, p. 21, 2011.

[28] K. Englehart and B. Hudgins, "A robust, real-time control scheme for multifunction myoelectric control," *IEEE Trans. Biomed. Eng.*, vol. 50, no. 7, pp. 848–854, Jul. 2003.

[29] T. R. Farrell and R. Weir, "A comparison of the effects of electrode implantation and targeting on pattern classification accuracy for prosthesis control," *IEEE Trans. Biomed. Eng.*, vol. 55, no. 9, pp. 2198–2211, Sep. 2008.

[30] S. Bhattacharya, A. Luo, T. K. Maiti, S. Dutta, Y. Ochi, M. Miura-Mattausch, and H. Jurgen Mattausch, "Surface-property recognition with force sensors for stable walking of humanoid robot," *IEEE Access*, vol. 7, pp. 146443–146456, 2019.

[31] Y. Huang, K. B. Englehart, B. Hudgins, and A. D. C. Chan, "A Gaussian mixture model based classification scheme for myoelectric control of powered upper limb prostheses," *IEEE Trans. Biomed. Eng.*, vol. 52, no. 11, pp. 1801–1811, Nov. 2005.

[32] M. T. Hoang, Y. Zhu, B. Yuen, T. Reese, X. Dong, T. Lu, R. Westendorp, and M. Xie, "A soft range limited K-nearest neighbors algorithm for indoor localization enhancement," *IEEE Sensors J.*, vol. 18, no. 24, pp. 10208–10216, Dec. 2018.

[33] H. Gan, M. H. B. M. Khir, G. W. B. Djaswadi, and N. Ramli, "A hybrid model based on constraint OSELM, adaptive weighted SRC and KNN for large-scale indoor localization," *IEEE Access*, vol. 7, pp. 6971–6989, 2019.

[34] L. Jiao, X. Geng, and Q. Pan, "BP*k* NN: *k*-Nearest neighbor classifier with pairwise distance metrics and belief function theory," *IEEE Access*, vol. 7, pp. 48935–48947, 2019.

[35] S. Bhattacharya, A. Luo, T. K. Maiti, S. Dutta, M. Miura-Mattausch, and H. J. Mattausch, "Fast recognition and control of walking mode for humanoid robot based on pressure sensors and nearest neighbor search," in *Proc. Int. Symp. Intell. Signal Process. Commun. Syst. (ISPACS)*, Nov. 2018, pp. 331–334.

SANDIP BHATTACHARYA received the Ph.D. (Eng.) degree from the Indian Institute of Engineering Science and Technology (IIEST), India, in 2017. He is currently working as a Postdoctoral Researcher with the HiSIM Research Center, Hiroshima University, Japan. His current research interests include nano device, interconnect modeling, and intelligent circuit design for robotics.

AIWEN LUO received the B.Eng. degree from Beijing Jiaotong University, in 2009, the M.Eng. degree from Jinan University, China, in 2012, and the D.Eng. degree from Hiroshima University, Japan, in March 2018. From April 2018 to August 2019, she worked as a Postdoctoral Researcher with Hiroshima University. She currently works with Jinan University, the University of Macau, and Hiroshima University. Her research interests include hardware-oriented computer vision, pattern recognition, and intelligent robotics.

S. Bhattacharya *et al.*: Force-Sensor-Based Surface Recognition With Surface-Property-Dependent Walking-Speed Adjustment

IEEE *Access*

SUNANDAN DUTTA received the M.Tech. degree from the Indian Institute of Engineering Science and Technology (IIEST), Shibpur, India, in 2017. He is currently pursuing the Ph.D. degree with the Graduate School of Engineering, Hiroshima University, Japan. His research interest includes the areas of humanoid robotics and system cybernetics.

MITIKO MIURA-MATTAUSCH (Fellow, IEEE) received the D.Sc. degree from Hiroshima University, Japan. Since 1996, she has been a Professor with Hiroshima University, where she is leading the Ultra-Scaled Device Laboratory.

HANS JÜRGEN MATTAUSCH (Senior Member, IEEE) received the Ph.D. degree from Stuttgart University, Stuttgart, Germany. Since 1996, he has been a Professor with Hiroshima University, Japan, where he is involved in researching on very large-scale integration design, nano-electronics, and compact modeling.

● ● ●